Atomic-phase interference devices based on ring-shaped Bose-Einstein condensates: Two-ring case

B. P. Anderson,[1] K. Dholakia,[2] and E. M. Wright[1,2,*]
[1]*Optical Sciences Center, University of Arizona, Tucson, Arizona 85721*
[2]*School of Physics & Astronomy, University of St Andrews, North Haugh, St Andrews, Fife KY16 9SS, Scotland, United Kingdom*
(Received 12 September 2002; published 11 March 2003)

We theoretically investigate the ground-state properties and quantum dynamics of a pair of adjacent ring-shaped Bose-Einstein condensates that are coupled via tunneling. This device, which is the analog of a symmetric superconducting quantum interference device, is the simplest version of what we term an atomic-phase interference device (APHID). The two-ring APHID is shown to be sensitive to rotation.

DOI: 10.1103/PhysRevA.67.033601 PACS number(s): 03.75.Hh

I. INTRODUCTION

The last few years have witnessed magnificent advances in the preparation, manipulation, and exploration of atomic Bose-Einstein condensates (BECs). These quantum-degenerate systems offer an excellent experimental platform from which to study a multitude of nonlinear matter-wave phenomena including four-wave mixing [1], dark [2] and bright [3] solitons, superfluid vortices [4], and the generation and study of quantized vortices on toroidal atomic traps or rings. In particular, ring-shaped BECs allow for the study of phenomena related to persistent currents and rotational motion, with potential applications to rotation sensing. In this paper, our goal is to take the first theoretical steps in studying Josephson coupling between adjacent ring BECs (as opposed to concentric ring BECs that have been considered previously [5]). In particular, we investigate how quantum tunneling between two condensates trapped in adjacent toroidal traps, formed, for example, using optical-dipole traps with Laguerre-Gaussian light beams, modifies both the ground-state properties and quantum dynamics of the system. The two-ring BEC system is the simplest example of what we refer to as an atomic-phase interference device (APHID), essentially a neutral-atom analog of a superconducting quantum interference device (SQUID). The properties of the APHID will be shown to be strongly influenced by the individual phases of the matter-waves in the rings.

The remainder of this paper is organized as follows: In the following section we elucidate the details of the model we use. Following this, we explore the properties of the ground state and the first-excited state of the system. We then look at the Josephson coupling and the time-dependent solutions, highlighting important considerations due to the effects of rotation, followed by concluding remarks.

II. BASIC MODEL

The basic model we consider is shown in Fig. 1(a) and comprises two identical ring BECs labeled $j=1$, 2, which are in close proximity, and the whole system is rotating at an angular frequency ω_R around the z axis, which is pointing out of the page. The close proximity of the rings allows for spatially dependent tunneling between them via mode overlap, meaning that the rings are coupled, allowing Josephson oscillations [6,7]. Each individual ring may be realized physically, using a toroidal trap of high aspect ratio $R=L/\ell_0$, where L is the toroid circumference and ℓ_0 the transverse oscillator length, $\ell_0=\sqrt{\hbar/m\omega_0}$, with ω_0 the frequency of transverse oscillations, assumed to be harmonic. The transverse trap potential is assumed to be symmetric about an axis consisting of a circle on which the trap potential is minimum. The longitudinal (circumferential) motion on each ring can be described approximately by a one-dimensional (1D) coordinate $x_j \in [-L/2, L/2]$ obtained by unfolding the ring and applying periodic boundary conditions, as illustrated in Fig. 1(b). Then, at zero temperature the quantum dynamics of an atomic BEC moving on the paired rings may be described by the following coupled Gross-Pitaevskii equations in a reference frame rotating at ω_R [8–11]:

$$i\hbar\frac{\partial\psi_j}{\partial t}=\hbar\omega_0\psi_j-\frac{\hbar^2}{2m}\frac{\partial^2\psi_j}{\partial x^2}-i(-1)^j\frac{\hbar\omega_R L}{2\pi}\frac{\partial\psi_j}{\partial x}+g|\psi_j|^2\psi_j+\hbar\Omega(x)\psi_{3-j}, \quad (1)$$

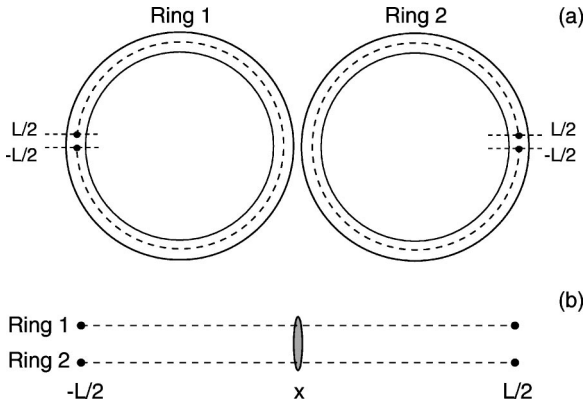

FIG. 1. (a) The basic model we consider comprises two identical ring BECs labeled $j=1,2$ which are in close proximity and coupled via tunneling, and (b) shows the unfolded rings to which periodic boundary conditions are applied. The rings come closest together at the origin $x=0$, where tunneling is represented by a dark oval. The whole system rotates at an angular velocity ω_R about the z axis pointing out of the page.

*Email address: ewan.wright@optics.arizona.edu

where $\psi_j(x,t)$ is the macroscopic wave function for ring $j=1,2$, with normalization condition

$$\int_{-L/2}^{L/2} dx[|\psi_1(x,t)|^2+|\psi_2(x,t)|^2]=N. \tag{2}$$

Here, N is the number of atoms of mass m, $g=4\pi\hbar^2 a/(2\pi\ell_0^2 m)=2\hbar\omega_0 a>0$ is the effective one-dimensional nonlinear coefficient describing repulsive many-body interactions, a being the s wave scattering length, and $\Omega(x)>0$, which is chosen real and positive, is the spatially dependent tunneling frequency between the two rings. In writing Eqs. (1) we have taken advantage of the fact that although the atoms in each ring are described by different coordinates $x_{j=1,2}$, they can nonetheless be described as moving on the same domain $x\in[-L/2,L/2]$ with the caveat that the atoms on each ring do not cross interact via mean-field effects, and are only coupled via the spatially dependent tunneling.

The third term on the right-hand side of Eqs. (1) arises from the rotation of the whole system at frequency ω_R around the z-axis. In particular, we have used the result [12] that in the rotating frame of reference the Hamiltonian of the system is given by $H'=H-\vec{\Omega}\cdot\vec{L}=H-\omega_R L_z$, where H is the Hamiltonian of the nonrotating system, $\vec{\Omega}=\omega_R\vec{z}$ is the angular velocity vector directed along the z axis, and $\vec{L}$ is the vector angular momentum operator of the atoms trapped on each ring. We may express the circumferential coordinate x around the ring as an angular variable $\theta=2\pi x/L$, in terms of which the z component of the angular momentum operator is $L_z=-i\hbar\partial/\partial\theta$, so that $H'=H+i(\hbar\omega_R L/2\pi)\partial/\partial x$. However, inspection of Figs. 1(a) and 1(b) shows that atoms circulating from $x=-L/2\rightarrow L/2$ along ring $j=1$ are going counterclockwise, whereas atoms circulating from $x=-L/2\rightarrow L/2$ along ring $j=2$ are going clockwise. This means that although we write the equations using a common spatial coordinate $x=(\theta/2\pi)L\in[-L/2,L/2]$, propagation in a given x direction corresponds to opposite senses of rotation the different rings. This is why the third term in Eqs. (1), $-i(-1)^j(\hbar\omega_R L/2\pi)\partial\psi_j/\partial x$, describing the rotation of the whole system, has a ring-dependent sign $(-1)^j$.

With reference to Fig. 1(a) we see, for example, that for an atom moving clockwise from a given reference point on ring $j=1$, then tunneling over to ring $j=2$ and moving counterclockwise, and finally tunneling back after orbiting ring $j=2$ to ring $j=1$ to the original starting point, the atom crosses the tunneling region twice. In this sense the coupled atomic rings are analogous to a symmetric SQUID [6], in which two superconducting rings are connected by a weak link, which has been employed as a magnetometer [13]. The two-ring system, then, is the simplest version of an APHD, and we concentrate on the two-ring case in this paper to explore the basic properties of the APHIDs.

The tunneling frequency $\Omega_{max}=\Omega(x=0)$ will be at its maximum at the point of closest approach of the rings, which we choose at $x=0$, and will decrease with separation, or equivalently as x varies away form the origin. Typically, the tunneling frequency decays exponentially with ring separation. Thus, $\Omega(x)$ will generically be a bell-shaped function of x, and the spatial extent of the Josephson coupling will be much less than the size of ring L. Clearly, for smaller rings with tighter curvature, $\Omega(x)$ will drop off faster away from the peak. In the limit $\Omega(x)=0$, Eqs. (1) reduce to the approximate one-dimensional form previously used to describe atomic BECs on a toroid [9–11].

The conserved N-particle energy functional for the coupled Gross-Pitaevskii equation (1) is

$$E=N\hbar\omega_0+\int_0^L dx\left[\frac{\hbar^2}{2m}\left(\left|\frac{\partial\psi_1}{\partial x}\right|^2+\left|\frac{\partial\psi_2}{\partial x}\right|^2\right)+i\frac{\hbar\omega_R L}{2\pi}\left(\psi_2^*\frac{\partial\psi_1}{\partial x}-\psi_1^*\frac{\partial\psi_2}{\partial x}\right)+\frac{g}{2}(|\psi_1|^4+|\psi_2|^4)+\hbar\Omega(x)(\psi_1\psi_2^*+\psi_1^*\psi_2)\right], \tag{3}$$

giving the energy per particle $\epsilon=E/N$. Since in this paper the transverse confinement energy $\hbar\omega_0$ is assumed the same for both the rings and simply redefines the zero of energy, we hereafter drop this energy term for simplicity in notation.

III. GROUND AND FIRST-EXCITED STATES

In this section we examine the properties of the ground and first-excited states of a nonrotating ($\omega_R=0$) pair of coupled ring BECs, using a simple model to expose the main features.

A. Zero-coupling limit

It is useful in assessing the ground-state properties to consider the noncoupled case with $\Omega(x)=0$. If all N atoms are homogeneously distributed on just one of the rings, with $\psi_j=\sqrt{N/L}$ and $\psi_{3-j}=0$, then according to Eq. (3) the energy per particle is $\epsilon_{trap}=gn/2$, where $n=N/L$ is the linear atomic density. In contrast, when the atoms are equally split between the two rings, but still homogeneously distributed on each ring, $|\psi_j|=\sqrt{N/2L}$, and the energy per particle is

$$\epsilon_{1/2}=\frac{gn}{4}, \tag{4}$$

irrespective of the relative phase between the macroscopic wave functions of the two rings. Energetically speaking then, in the absence of coupling the lowest-energy state is that in which the atoms are equally split between the rings, as this minimizes the mean-field energy.

B. Coupled solutions

To proceed we now reintroduce the coupling and look for solutions where the atoms are equally split between the rings. In particular, we consider solutions where the macroscopic wave functions of the two rings are in phase $(+)$ and out of phase $(-)$ by making the ansatz

$$\psi_j(x,t)=\frac{(\pm 1)^j}{\sqrt{2}}e^{-i\mu_\pm t/\hbar}\varphi_\pm(x), \quad j=1,2, \tag{5}$$

with $\varphi_\pm(x)$ the mode profiles on each ring and $\mu_\pm$ the corresponding chemical potentials. Then substituting in Eqs. (1) we obtain

$$\mu_\pm\varphi_\pm=-\frac{\hbar^2}{2m}\frac{d^2\varphi_\pm}{dx^2}+\frac{g}{2}|\varphi_\pm|^2\varphi_\pm\pm\hbar\Omega(x)\varphi_\pm, \tag{6}$$

and $\int dx|\varphi_\pm(x)|^2=N$. On general grounds, the out-of-phase $(-)$ solution corresponds to the ground state. This can be seen from Eq. (6) where the spatially dependent coupling $\Omega(x)>0$, which is typically bell-shaped, plays the role of a confining (deconfining) potential for the out-of-phase (in-phase) solution, thereby allowing for lower energy in comparison to the case without coupling.

In the limit $\Omega=0$, Eq. (6) also has the well-known dark soliton solution [14–19] on the infinite domain $L\to\infty$,

$$\varphi_\pm(x)=\varphi_0(x)=\sqrt{n}\tanh\left(\frac{(x+x_0)}{\sqrt{2}x_h}\right), \tag{7}$$

with $\mu_0=gn/2$, where n is the linear density of the background (in the thermodynamic limit, where $N\to\infty$ and $L\to\infty$, $N/L\to n$ remains nonzero). The healing length x_h is derived from the relation

$$\frac{\hbar^2}{2mx_h^2}=\frac{gn}{2}. \tag{8}$$

The dark soliton solution represents a flat background density profile with a hole of width $x_h\ll L$ located at $x=-x_0$, at which a phase jump of π also occurs as φ_0 goes through zero. In the thermodynamic limit the energy per particle associated with the dark soliton solution calculated using Eq. (3) is $\epsilon_0=ng/4=\epsilon_{1/2}$, that is, it is the same as that in Eq. (4) for a homogeneous density on each ring without coupling. This arises because in the thermodynamic limit $x_h/L\to 0$, meaning that any energy increase due to the hole in the density makes a negligible effect on average; in other words, the hole in the density occupies a vanishingly small portion of the ring.

C. Analytic approximation

In general, numerical methods are required to solve Eq. (6) for the given parameters and tunneling profile $\Omega(x)$. In order to obtain insight into the ground-state properties, we employ a simple model

$$\Omega(x)=\Omega_{max}d\,\delta(x), \tag{9}$$

where Ω_{max} is the maximum tunneling frequency and d is the length of the tunneling region. This δ-function approximation will apply when d is much less than any other characteristic length scale of the problem, namely, ring length L and healing length x_h. For the stationary coupled-ring solutions described by Eq. (6), where $\Omega(x)$ plays the role of a single-particle potential, the δ function approximation yields a quantum-contact interaction [20]. Substituting Eq. (9) in Eq. (6) and integrating from $x=0_-$ to $x=0_+$ across the junction, we find that the action of the δ function coupling is equivalent to a condition on the macroscopic wave function derivative

$$\frac{\hbar^2}{2m}\left(\left.\frac{d\varphi_\pm}{dx}\right|_{x=0_+}-\left.\frac{d\varphi_\pm}{dx}\right|_{x=0_-}\right)=\pm\hbar\Omega_{max}d\varphi_\pm(0). \tag{10}$$

In the limit $L\gg x_h\gg d$, we further impose the condition that $\varphi_\pm(x)$ is symmetric around $x=0$ in order to satisfy the periodic ring boundary conditions, and we approximate

$$\varphi_\pm(x)\approx\sqrt{n}\tanh\left(\frac{x+x_\pm}{\sqrt{2}x_h}\right), \quad x>0. \tag{11}$$

With this approximation there is a cusp in $\varphi_\pm(x)$ at x=0, and the solution is extended to $x<0$ by imposing reflection symmetry around the origin. We can solve for the variables $x_\pm$ by substituting the approximate solution (11) in the boundary condition (10), which yields

$$\pm\hbar\Omega_{max}d=\left(\frac{\hbar^2}{m\sqrt{2}x_h}\right)\frac{[1-\tanh^2(x_\pm/\sqrt{2}x_h)]}{\tanh(x_\pm/\sqrt{2}x_h)}. \tag{12}$$

Since $\Omega_{max}>0$ we find by inspection that the in-phase solutions correspond to $x_+>0$ and the out-of-phase solutions to $x_-<0$. By introducing a dimensionless parameter $\zeta=x_+/\sqrt{2}x_h$, with $\zeta>0$ and $\zeta=x_-/\sqrt{2}x_h$, with $\zeta<0$, and using Eq. (8) for the healing length, we may write the above equation as

$$\frac{\hbar\Omega_{max}d}{g}=\sqrt{\frac{n}{2n_s}}\frac{[1-\tanh^2(\zeta)]}{\tanh(|\zeta|)}, \tag{13}$$

where $n_s=mg/\hbar^2$ is a scaled density. Figure 2 shows a plot

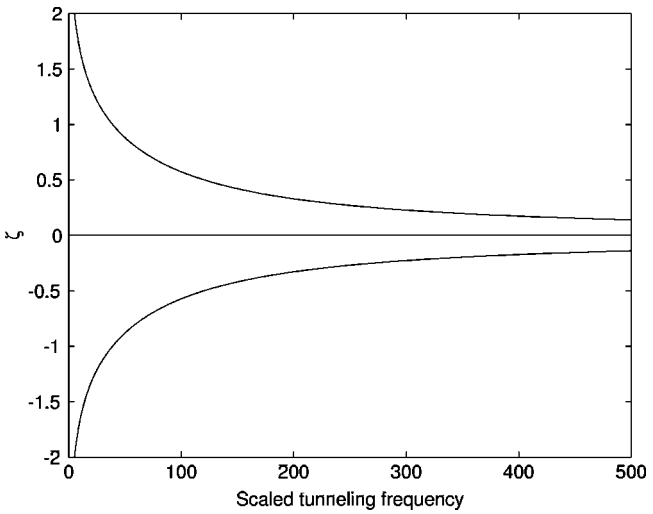

FIG. 2. Plot of ζ vs $\hbar\Omega_{max}d/g$ for $n/n_s=10^4$, with $\zeta=x_+/\sqrt{2}x_h$, $\zeta>0$, and $\zeta=x_-/\sqrt{2}x_h$, $\zeta<0$.

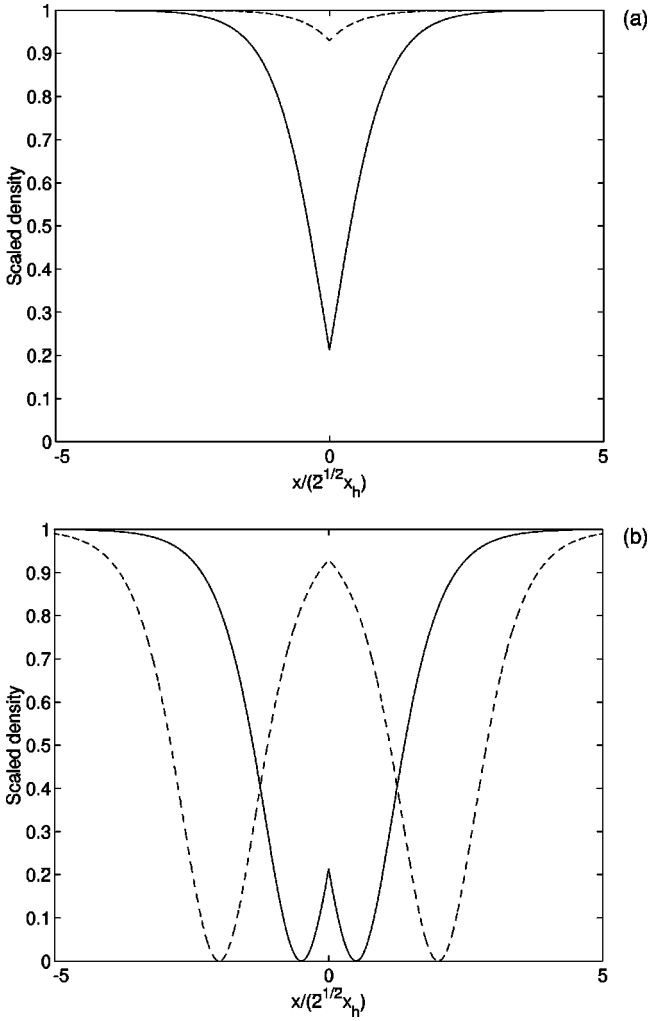

FIG. 3. Scaled density profiles $|\varphi_{\pm}|^2/n$ for $n/n_s=10^4$, $\hbar\Omega_{max}d/g=95,\zeta=0.5$ (solid lines), $\hbar\Omega_{max}d/g=6.3,\zeta=2$ (dashed lines): (a) the out-of-phase or ground-state solution and (b) the in-phase solution.

of ζ versus the scaled tunneling frequency $\hbar\Omega_{max}d/g$ for $n/n_s=10^4$. Figure 3 shows examples of scaled density profiles $|\varphi_{\pm}|^2/n$ for $\hbar\Omega_{max}d/g=95,\zeta=0.5$ (solid lines), $\hbar\Omega_{max}d/g=6.3,\zeta=2$ (dashed lines) and (a) the out-of-phase or ground-state solution, and (b) the in-phase solution. Density cusps in the solutions are evident, though we note that the ground-state density does not extend down to zero. The key features of the ground state are that as the scaled tunneling frequency $\hbar\Omega_{max}d/g$ is increased the depth of the density profile increases, the density at the origin going to zero as $\hbar\Omega_{max}d/g\rightarrow\infty$, and the width of the density hole also increases, approaching x_h as $\hbar\Omega_{max}d/g\rightarrow\infty$. The in-phase solution is different in that it displays two density zeros and an on-axis maximum, that is, a cusp, as shown in Fig. 3(b). Furthermore, inspection of the in-phase solution shows that its sign reverses through each density zero, and there are two sign reversals around each ring to ensure that the wave functions are single valued. The in-phase solution, therefore, has a phase structure like a pair of dark solitons on each ring. For smaller values $\hbar\Omega_{max}d/g$, the density zeros are spatially

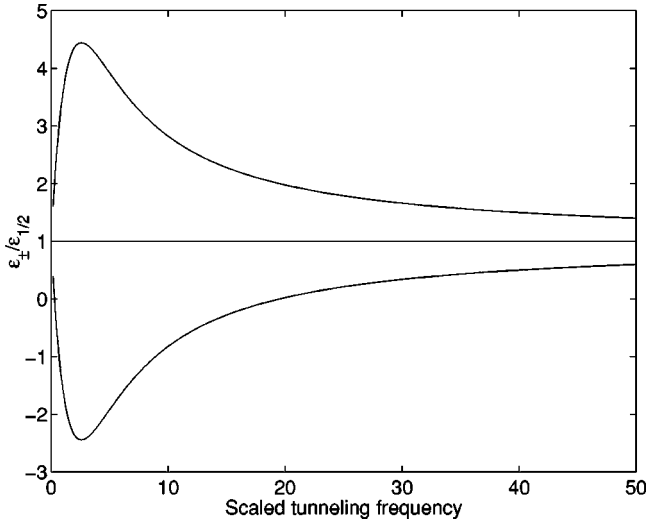

FIG. 4. Scaled energy per particle $\epsilon_{\pm}/\epsilon_{1/2}$ vs $\hbar\Omega_{max}d/g$ for $n/n_s=10$, the upper solid line corresponding to the in-phase $(+)$ solution and the lower solid line corresponding to the out-of-phase $(-)$ or ground-state solution.

separated [dashed line in Fig. 3(b) for $\hbar\Omega_{max}d/g=6.3,\zeta=2$], but come together at the origin as $\hbar\Omega_{max}d/g\rightarrow\infty$ [solid line in Fig. 3(b) for $\hbar\Omega_{max}d/g=95,\zeta=0.5$]. Thus, for both the in-phase and out-of-phase solutions the density vanishes at the origin as $\hbar\Omega_{max}d/g\rightarrow\infty$, and we have

$$\varphi_{\pm}(x)\approx\sqrt{n}\tanh\left(\frac{x}{\sqrt{2}x_h}\right). \tag{14}$$

A quantity of physical interest here is the energy per particle $\epsilon_{\pm}$ for the two solutions. Using the above approximate solution in the energy functional (3) we find in the thermodynamic limit

$$\epsilon_{\pm}=\frac{ng}{4}\pm\hbar\Omega_{max}dn\,\tanh^2(|\zeta|), \tag{15}$$

where the solution is again parametrized by ζ. Note that in the limit of zero coupling $\Omega_{max}\rightarrow 0$, the energies per particle of the two solutions become the same and equal to that of the equally split solution $\epsilon_{1/2}=ng/4$ as they should. Using Eq. (13) in Eq. (15) we obtain finally

$$\epsilon_{\pm}=\epsilon_{1/2}\left(1\pm\sqrt{\frac{8n}{n_s}}\tanh(|\zeta|)[1-\tanh^2(\zeta)]\right), \tag{16}$$

which is once again parametrized by ζ. Figure 4 shows $\epsilon_{\pm}/\epsilon_{1/2}$ versus $\hbar\Omega_{max}d/g$ for $n/n_s=10$, the upper solid line corresponding to the in-phase $(+)$ solution and the lower solid line to the out-of-phase $(-)$ or ground state solution. For small values of the scaled tunneling frequency $\hbar\Omega_{max}d/g<1$, the energy per particle for the in-phase (out-of-phase) solution initially increases (decreases) away from $\epsilon_{1/2}$ for zero-coupling, and this is expected physically. However, as the scaled tunneling frequency is increased further the energy per particle for the in-phase (out-of-phase) solution reaches a turning point at $\hbar\Omega_{max}d/g\approx 2$, then decreases

(increases), and both $\epsilon_{\pm}$ tend back to the zero-coupling value $\epsilon_{1/2}$ for $\hbar\Omega_{max}d/g\to\infty$. The reason for this is that, as discussed above, for both solutions the density tends to zero at the origin $x=0$ where the junction is concentrated in the limit $\hbar\Omega_{max}d/g\to\infty$, so the Josephson coupling is rendered inoperative and the energy per particle tends to that for zero coupling.

IV. TIME-DEPENDENT SOLUTIONS

A. Scaled equations

For purposes of numerical simulations we introduce a simple Gaussian model for the spatially dependent Josephson coupling

$$\Omega(x)=\Omega_{max}e^{-x^2/w^2}=\Omega_{max}df(x), \tag{17}$$

with Ω_{max} the maximum tunneling frequency and $w\ll L$ the width of the coupling region around $x=0$. We also introduce the normalized Gaussian $f(x)=\exp(-x^2/w^2)/\sqrt{\pi w^2}$ for which $d=\sqrt{\pi w^2}$ so that effective parameters can be compared with that of the preceding section. Then introducing the scaled variables

$$\tau=t(ng/\hbar),\quad \xi=x/L,\quad \psi_j=\sqrt{n}\phi_j, \tag{18}$$

with $n=N/L$ the mean density as before, we obtain with $j=1,2$,

$$i\frac{\partial\phi_j}{\partial\tau}=-\frac{\beta}{2}\frac{\partial^2\phi_j}{\partial\xi^2}-i(-1)^j\left(\frac{\nu}{2\pi}\right)\frac{\partial\phi_j}{\partial\xi}+|\phi_j|^2\phi_j+\eta e^{-\xi^2/\Delta^2}\phi_{3-j}, \tag{19}$$

where $\int d\xi[|\phi_1|^2+|\phi_2|^2]=1$ and

$$\Delta=\frac{w}{L}\ll 1,\quad \eta=\frac{\hbar\Omega_{max}}{ng},\quad \nu=\frac{\hbar\omega_R}{ng},\quad \beta=\frac{n/n_s}{N^2}. \tag{20}$$

These are the scaled equations used for our numerical study. We have solved the equations numerically using the split-step fast-Fourier transform method [21].

To study the quantum dynamics of the coupled-ring BECs, we shall use an initial condition at $\tau=0$, where all N atoms are on one ring in a vortex state of winding number p. This may be realized, for example, by condensing the atoms on one ring in the absence of the other, stirring the BEC to create the vortex [22], and then turning on the second ring. Sauer *et al.* [23] have demonstrated a 2-cm diameter magnetic storage ring for laser-cooled, and Arnold and Riis [24] have worked towards realizing a 10-cm diameter magnetically trapped toroidal BEC. One scheme for turning rings off and on is to use toroidal optical dipole traps [25] formed by Laguerre-Gaussian beams piercing a two-dimensional BEC to create the rings [5,26,27], or alternatively using scanned laser beams to form the toroidal traps [28]. Cavity field enhancement may also be used to allow for large-radius toroidal traps [29]. Regardless of experimental method, the initial condition we take is

$$\phi_1(\xi,0)=e^{2\pi ip\xi},\quad \phi_2=0. \tag{21}$$

B. Resonance conditions

To proceed we examine the resonance conditions leading to the initial exchange of atoms from ring $1\to 2$, using first-order perturbation theory. For the initial condition (21) we choose the zeroth-order solution as that for $\nu=0$,

$$\phi_1^{(0)}(\xi,\tau)=e^{2\pi ip\xi}e^{-i(2\pi^2\beta p^2-p\nu+1)\tau}. \tag{22}$$

Then writing the first-order solution for ring 2 in the form

$$\phi_2^{(1)}(\xi,\tau)=\sum_{q=-\infty}^{\infty}a_q(\tau)e^{2\pi iq\xi}e^{-i(2\pi^2\beta q^2+q\nu)\tau} \tag{23}$$

yields

$$|a_q(\tau)|^2=4\eta^2\mathcal{F}_{pq}^2\frac{\sin^2(\chi_{pq}\tau/2)}{\chi_{pq}^2}, \tag{24}$$

where

$$\mathcal{F}_{pq}=\sqrt{\pi}\Delta e^{-\pi^2\Delta^2(p-q)^2},$$
$$\chi_{pq}=2\pi^2\beta(p^2-q^2)-\nu(p+q)+1. \tag{25}$$

The vortex states q of ring 2 are therefore excited and generally exhibit small oscillations except at the resonance where χ_{pq} becomes small. The level of excitation of the qth vortex state is also dictated by the factor $\mathcal{F}_{pq}$, but since we assume a narrow junction, $w/L=\Delta\ll 1$, this factor allows for almost constant excitation, $\mathcal{F}_{pq}\approx\sqrt{\pi}\Delta$, in the range $q=p\pm\delta q$ with

$$\delta q=\frac{1}{\pi\Delta}\gg 1. \tag{26}$$

Consider first the case that the system is not rotating, $\nu=0$: Resonance occurs for that integer value of q_r for which χ_{pq} is equal to or closest to zero:

$$q_r^2=p^2+\frac{1}{2\pi^2\beta}, \tag{27}$$

the width of the resonance being

$$\Delta q\approx\frac{1}{2\pi^2(p+q_r)\beta}. \tag{28}$$

When the width of the resonance is small, $\Delta q<1$, the initial vortex of index p in ring 1 will selectively couple to vortices with mode indices q_r satisfying Eq. (27) in ring 2, giving rise to a few relatively simple mode dynamics. In contrast, when $\Delta q\gg 1$ the initial vortex of index p in ring 2 will couple to a

broad range of vortices with mode indices $q_r \pm \Delta q$ in ring 2, giving rise to multimode dynamics and complex behavior. In addition, for Josephson oscillations to occur the tunneling energy per particle averaged over the ring length $(1/L)\int dx \hbar\Omega(x) = \hbar\Omega_{max}\sqrt{\pi}w/L$ should be of the same order as the mean-field energy per particle ng, or

$$\eta = \frac{\hbar\Omega_{max}}{ng} \sim \frac{1}{\sqrt{\pi}\Delta}. \tag{29}$$

This gives an estimate of the scaled tunneling frequency η to obtain Josephson oscillations.

C. Numerical results

Here we present some examples of the dynamics of the coupled-ring BECs. For all the simulations we set $p=0, \Delta = 10^{-2}$, and $\eta = 50$. Consider first that the initial state corresponds to the ground state ($p=0$) of ring 1. From Eqs. (27) and (28) we obtain

$$q_r = \sqrt{\frac{1}{2\pi^2\beta}} = \Delta q, \tag{30}$$

that is, the width of the resonance Δq is equal to the resonant value $q = q_r$. Figure 5(a) shows the fraction of atoms in each ring for $\beta = 1$ for which $q_r = \Delta q = 0.22$, and complete Josephson oscillations between the two rings are evident. In this case the density profiles in the two rings are largely flat as resonant coupling occurs between the individual modes in each ring with $p=0, q_r \approx 0$. In contrast, for $\beta = 5.1\times 10^{-2}$, as shown in Fig. 5(b) for which $q_r = \Delta q = 1$, the Josephson oscillations are now incomplete. Physically, there are multiple spatial modes involved in ring $j=2$ with $q = 0, \pm 1, \pm 2$, and the resulting multimode dynamics is what frustrates the Josephson oscillations for $\Delta q \geqslant 1$. The multimode dynamics manifests itself as spatial density modulations in the two rings as shown in Fig. 6(a), for the same parameters as in Fig. 5(b) and $\tau = 10$. For even lower density $\beta = 5.1\times 10^{-4}$ for which $q_r = \Delta q = 10$, the Josephson oscillations are all but extinguished, and the spatial density profiles in rings $j = 1,2$ are shown in Fig. 6(b) for $\tau = 10$. We remark that the rapid spatial oscillations in Fig. 6(b) are not numerical noise, and the calculation is well resolved numerically and is reproducible; rather, the density modulations are the signature that the dynamics now involves many spatial modes with $q = 0, \pm 1, \pm 2, \ldots$. In particular, the multimode nature of the solution allows the coupling due to tunneling to concentrate around the coupling region, that is, only atoms in the immediate vicinity of the coupling region participate in tunneling, hence reducing the maximum fraction of atoms that can be transferred between the rings. This is illustrated in Fig. 6(b) where the density in ring 2 (bold line), and hence the coupling to ring 2, is concentrated around the origin and is close to zero away from the coupling region.

Some estimates of parameters are in order. Using $g = 2\hbar\omega_0 a$ gives $ng = 2\hbar\omega_0 N(a/L)$, and $\Omega_{max} = 2\eta\omega_0 N(a/L)$. Then for $\omega_0 = 2\pi\times 10^2$ rad s^{-1}, $N = 10^3$, $L = 1$ cm, $a = 5$ nm, we find $\Omega_{max} = 2\pi\times 5$ rad s^{-1}, and τ is time in units of $\hbar/ng = 1.6$ s, so the Josephson oscillations in Fig. 5(a) occur on a time scale of seconds. Setting $m = 10^{-25}$ kg we obtain $n_s = mg/\hbar^2 \approx 63$ cm^{-1}, and for $n = N/L = 10^3$ cm^{-1}, $\beta = 1.6\times 10^{-5}$. It is important that $n/n_s > 1$ to ensure that the one-dimensional gas acts as a BEC as opposed to a Tonks gas [30,31]. The parameter $\beta = (n/n_s)/N^2$ is proportional to $1/\omega_0$ and $1/N$, so we can increase β by decreasing either the number of atoms and/or the transverse oscillator frequency with respect to the above values.

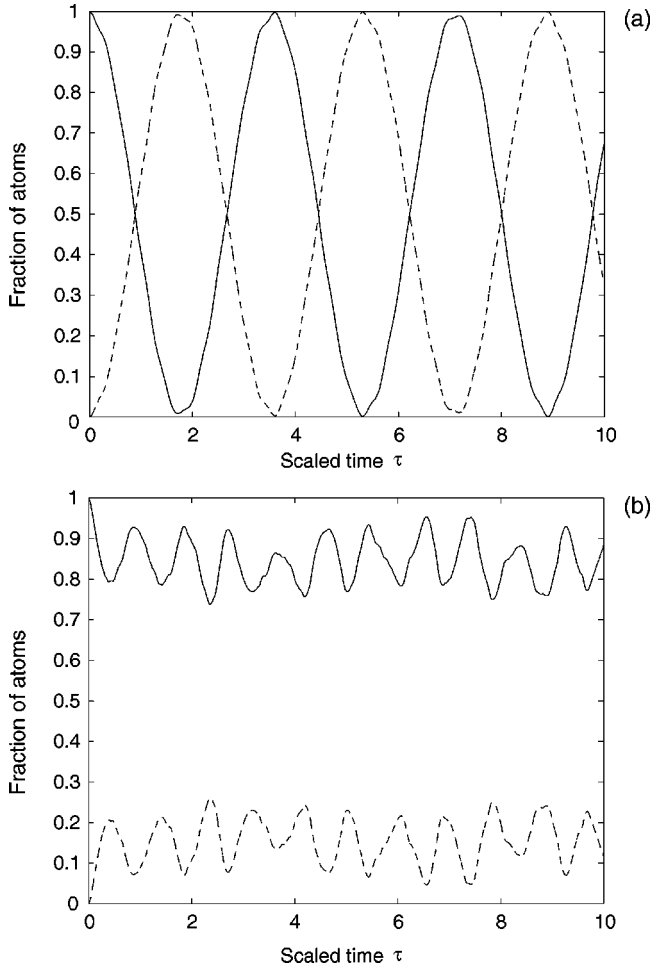

FIG. 5. Fraction of atoms in each ring for $\Delta = 10^{-2}$, $\eta = 50$: (a) $\beta = 1, \Delta q = 0.22$ and (b) $\beta = 5.1\times 10^{-2}, \Delta q = 1$.

D. Effects of rotation

An interesting feature of the two-ring APHID is that the condition $\chi_{pq} = 2\pi^2\beta(p^2 - q^2) - \nu(p+q) + 1 \to 0$ for resonant coupling between the rings is dependent on the scaled rotation rate $\nu = \hbar\omega_R/ng$. In particular we find, for $p=0$,

$$q_r = \frac{1}{4\pi^2\beta}[-\nu \pm \sqrt{\nu^2 + 8\pi^2\beta}]. \tag{31}$$

This implies that for scaled rotation rates $|\nu| \sim \sqrt{8\pi^2\beta}$ the rotation of the entire APHID will affect the coupling. Con-

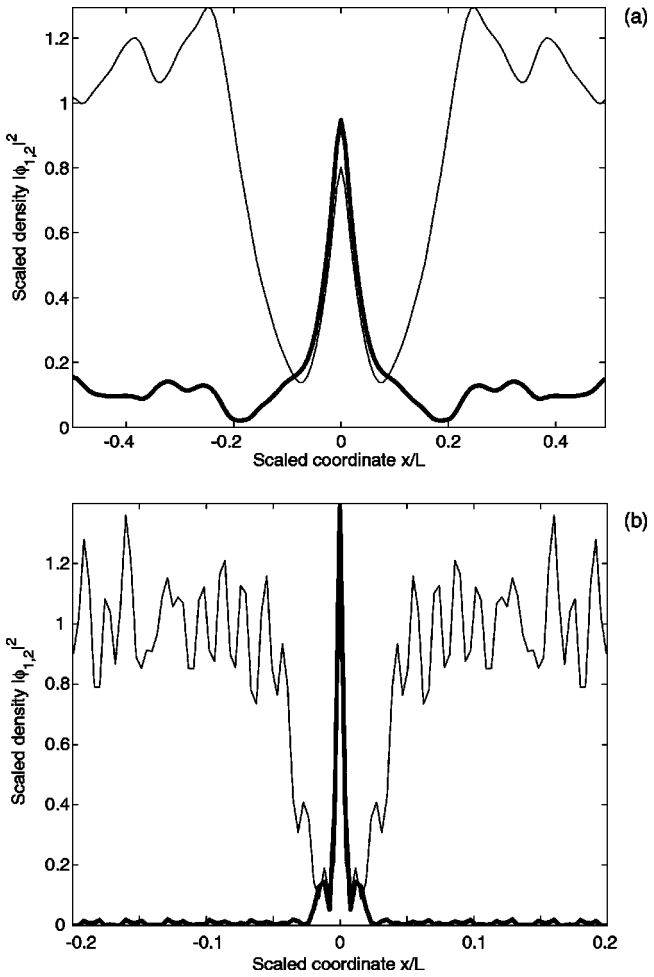

FIG. 6. (a) Spatial density in ring $j=1$ (thin line) and $j=2$ (bold line) for the same parameters as Fig. 5(b) with $\tau=10$, $\beta=5.1\times10^{-2}$, and $\Delta q=1$; (b) spatial density in ring $j=1$ (thin line) and $j=2$ (bold line) for $\beta=5.1\times10^{-4}$,$\Delta q=10$ for $\tau=10$, and on the range $x\in[-0.2L,0.2L]$ so that the density profiles can be resolved.

sider then a case where without rotation $\Delta q\gg1$ so that the Josephson oscillations are all but extinguished and the atoms remain on ring 1. Then as the scaled rotation rate ν is increased from zero, inspection shows that one solution q_r in Eq. (31) moves towards resonance, while the other moves further away. Therefore, starting from a detuned case with minimal coupling, increased rotation leads to increased coupling, which can then be detected via the number of atoms on ring 2 at a fixed-detection time. Physically, the tunnel-coupled rings are an example of coupled nonlinear oscillators, and it is well-known that the coupling between nonlinear oscillators is dependent upon any asymmetries between them that causes an energy mismatch between the oscillators. Equations (1) show that rotation of the whole system at an angular frequency ω_R affects the two rings differently, and this introduces an energy or phase mismatch between the two rings that can inhibit or enhance the coupling. For the initially detuned case considered here the rotation partially restores the coupling, and this manifests itself as a change in the number of coupled atoms in ring 2 due to the rotation.

Figure 7 shows the percentage of the atoms in ring 2

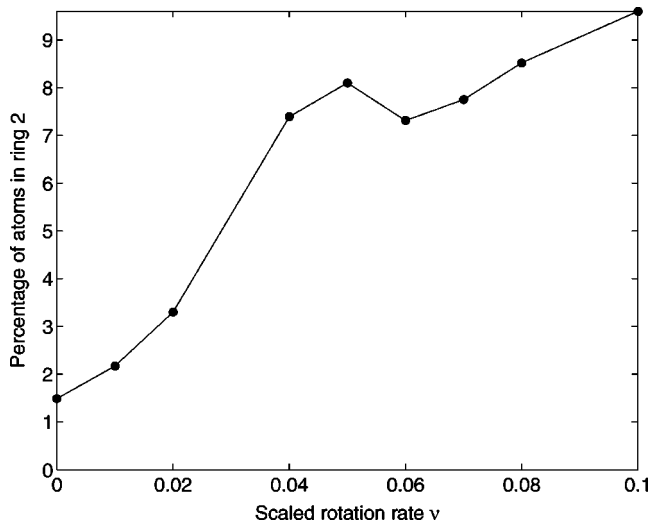

FIG. 7. Percentage of atoms in ring $j=2$ as a function of scaled rotation rate $\nu=\hbar\omega_R/ng$. The numerical data points are shown as circles and the solid line is included as an aid to the eye.

versus scaled rotation rate ν at time $\tau=10$ and $\Delta=0.01,\eta=50,\beta=5.1\times10^{-4}$, for which $q_r=\Delta q=10$, and the effect of rotation-dependent coupling between the rings is clearly exhibited (the numerical data points are shown as circles). Some points are worth making here: First, the rotation causes the number of atoms in ring 2 to change by about 10% of the total number of atoms, so experimentally it will be necessary to control the initial number of atoms on ring 1 to better than this percentage. Furthermore, it would be a challenge to detect the small number of atoms in ring 2. Second, for our particular example with $p=0$, the number of atoms in ring 2 is sensitive to the magnitude but not the sign of the rotation, but this can be changed by having $p\neq0$ in which case the coupling becomes sensitive to the sign of ν. Third, the sensitivity of the atom number to the rotation rate increases with the observation time τ chosen, remembering that we are in a far-off-resonant situation, so coupling happens slowly. Finally, the number of atoms in ring 2 is not necessarily a monotonic function of the rotation rate, as seen from Fig. 7, which will limit the range of rotation rates that can be uniquely measured. Nonetheless, we feel this is an interesting phenomena that may have utility for rotation sensing with further development.

To gain some sense of the sensitivity of this scheme we use the same parameters as the preceding section for which τ is the time in units of $\hbar/ng=1.6$ s. Then a value of $\nu=0.01$ corresponds to a rotation rate $\omega_R=2\nu\omega_0N(a/L)=2\pi\times10^{-3}$ rad s^{-1}, which is 100 times higher than the Earth's rotation rate at the poles. However, if we are willing to reduce the transverse oscillator frequency to $\omega_0=2\pi\times1$ rad s^{-1}, then $\nu=0.01$ corresponds to the Earth's rotation rate, but then the time is in units of 160 s in the figures! We are currently working on schemes involving multiple-ring APHIDs to enhance the rotation sensitivity.

V. SUMMARY AND CONCLUSIONS

In summary, we have presented a theoretical investigation of a pair of ring BECs coupled by tunneling as the simplest

example of a potential APHID. We have shown that the two-ring APHID has interesting ground-state properties, with density profiles reminiscent of dark soliton states around the point of contact of the rings. Furthermore, we have demonstrated that Josephson oscillations between the two rings can occur, and that these oscillations are sensitive to the state of rotation of the APHID. In particular, if all the atoms are prepared on one ring, then the number of atoms transferred to the second ring in a given time span is a measure of the rotation rate of the APHID. Although the two-ring APHID was found to be not very rotation sensitive, we believe APHIDs are worthy of further study as multiring APHIDs will display enhanced sensitivity to the relative phase between the rings, hence potentially leading to increased rotation sensitivity. We shall be exploring multiring APHIDs in future research.

ACKNOWLEDGMENTS

This work was supported by the Office of Naval Research Contract No. N00014-99-1-0806, the U.S. Army Research Office, and the Royal Society of Edinburgh. K.D. acknowledges the support of the U.K. Engineering and Physical Sciences Research Council.

[1] L. Deng, *et al.*, Nature (London) **398**, 218 (1999).
[2] S. Burger, *et al.*, Phys. Rev. Lett. **83**, 5198 (1999); J. Denschlag, *et al.*, Science **287**, 97 (2000).
[3] K.E. Strecker, *et al.*, Nature (London) **417**, 150 (2002).
[4] M.R. Matthews *et al.*, Phys. Rev. Lett. **83**, 2498 (1999); K.W. Madison *et al.*, *ibid.* **84**, 806 (2000).
[5] J. Tempere, J.T. Devreese, and E.R.I. Abraham, Phys. Rev. A **64**, 023603 (2001).
[6] D. R. Tilley and J. Tilley, *Superfluidity and Superconductivity*, 2nd ed. (Adam Hilger, Bristol, 1986), Chap. 7.
[7] J. Javanainen, Phys. Rev. Lett. **57**, 3164 (1986).
[8] E.M. Lifshitz and L.P. Pitaevskii, *Statistical Physics*, Part 2 (Pergamon Press, Oxford, 1989), pp. 85–118.
[9] D.S. Rokhsar, e-print cond-mat/9709212.
[10] J. Javanainen, S.M. Paik, and S.M. Yoo, Phys. Rev. A **58**, 580 (1998).
[11] M. Benakli, *et al.*, Europhys. Lett. **46**, 275 (1999).
[12] L.D. Landau and E.M. Lifshitz, *Statistical Physics*, Part 1 (Pergamon Press, Oxford, 1988), p. 74.
[13] J.E. Zimmerman, J. Appl. Phys. **41**, 1589 (1970).
[14] W.P. Reinhardt and C.W. Clark, J. Phys. B **30**, L785 (1997).
[15] R. Dum *et al.*, Phys. Rev. Lett. **80**, 2972 (1998).
[16] T.F. Scott, R.J. Ballagh, and K. Burnett, J. Phys. B **31**, L329 (1998).
[17] A.D. Jackson, G.M. Kavoulakis, and C.J. Pethick, Phys. Rev. A **58**, 2417 (1998).
[18] A.E. Muryshev *et al.*, Phys. Rev. A **60**, R2665 (1999).
[19] L.D. Carr *et al.*, Phys. Rev. A **62**, 063610 (2000).
[20] C. Trueman and K.K. Wan, J. Math. Phys. **41**, 195 (2000).
[21] J.A. Fleck, J.R. Morris, and M.D. Feit, Appl. Opt. **10**, 129 (1976).
[22] J. Brand and W.P. Reinhardt, J. Phys. B **34**, L113 (2001).
[23] J.A. Sauer, M.D. Barrett, and M.S. Chapman, Phys. Rev. Lett. **87**, 270401 (2001).
[24] A.S. Arnold and E. Riis, J. Mod. Opt. **49**, 959 (2002).
[25] D.M. Stamper-Kurn, *et al.*, Phys. Rev. Lett. **80**, 2027 (1998).
[26] L. Salasnich, A. Parola, and L. Reatto, Phys. Rev. A **59**, 2990 (1999).
[27] E.M. Wright, J. Arlt, and K. Dholakia, Phys. Rev. A **63**, 013608 (2000).
[28] Dallin S. Durfee, Ph.D. thesis, MIT, 1999 (unpublished).
[29] T. Freegarde and K. Dholakia, Opt. Commun. **201**, 99 (2002).
[30] M. Olshanii, Phys. Rev. Lett. **81**, 938 (1998).
[31] D.S. Petrov, G.V. Shlyapnikov, and J.T.M. Walraven, Phys. Rev. Lett. **85**, 3745 (2000).